

A Lightweight CNN and Joint Shape-Joint Space (JS^2) Descriptor for Radiological Osteoarthritis Detection

Neslihan Bayramoglu¹, Miika T. Nieminen^{1,2,3}, and Simo Saarakkala^{1,2,3}

¹ Research Unit of Medical Imaging, Physics and Technology, University of Oulu, Finland

² Department of Diagnostic Radiology, Oulu University Hospital, Oulu, Finland

³ Medical Research Center, University of Oulu and Oulu University Hospital, Oulu, Finland

Abstract. Knee osteoarthritis (OA) is very common progressive and degenerative musculoskeletal disease worldwide creates a heavy burden on patients with reduced quality of life and also on society due to financial impact. Therefore, any attempt to reduce the burden of the disease could help both patients and society. In this study, we propose a fully automated novel method, based on combination of joint shape and convolutional neural network (CNN) based bone texture features, to distinguish between the knee radiographs with and without radiographic osteoarthritis. Moreover, we report the first attempt at describing the bone texture using CNN. Knee radiographs from Osteoarthritis Initiative (OAI) and Multicenter Osteoarthritis (MOST) studies were used in the experiments. Our models were trained on 8953 knee radiographs from OAI and evaluated on 3445 knee radiographs from MOST. Our results demonstrate that fusing the proposed shape and texture parameters achieves the state-of-the art performance in radiographic OA detection yielding area under the ROC curve (AUC) of 95.21%.

Keywords: Knee osteoarthritis · Joint space width · Joint shape · Bone texture.

1 Introduction

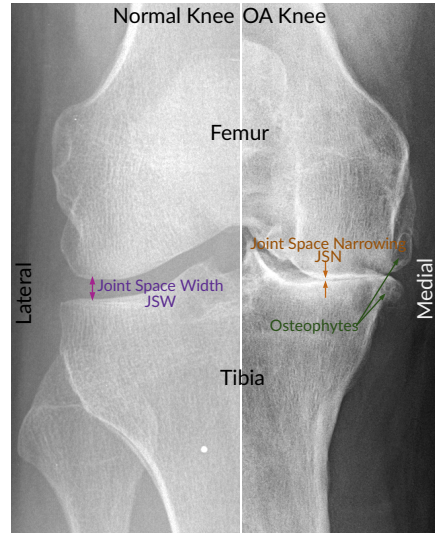
Osteoarthritis (OA) is one of the leading cause of disability around the world. The condition causes pain, stiffness, and limitations in movement. Several different risk factors have been identified for OA including age, obesity, injury, repetitive use of joints, bone density, muscle weakness, and gender [1]. The incidence of OA is steeply rising because of the ageing population [1]. OA, which is a disease of the developed world, creates a heavy burden on patients with reduced quality of life and also on society due to treatment costs and time off at work.

Although there is no cure for OA, its symptoms can be controlled by modifying the risk factors and with other conservative measures. Therefore, early identification and treatment of OA may be critical for decreasing the chronic

pain and improve joint function. It is also important to have a better understanding of the disease to develop new treatments to slow its progression and delay joint replacement surgery [2].

OA is currently diagnosed by clinical examination and, when necessary, with radiography (X-ray imaging) and other advanced imaging modalities such as MRI scanning and arthroscopy. Although conventional radiography (X-ray imaging) has several limitations [3], it is still the primary choice and the most widely used imaging modality in OA because it is more affordable and accessible than other imaging modalities [4]. X-Ray imaging allows for detection of characteristic features of OA including osteophyte formation, joint space narrowing, subchondral sclerosis, and cysts formation (Figure 1).

Fig. 1: Examples of X-ray images of normal knee and severe OA knee. The left side shows normal knee and the right side shows OA knee. In this image, in addition to the joint compartments, joint space narrowing (JSN) and osteophytes are demonstrated.



Several grading systems have been developed to evaluate the OA severity from knee radiographs in clinical practice; semi-quantitative Kellgren and Lawrence (KL) grading system being the most widely used [5]. In KL grading system, the grade varies from 0 to 4 correlating to increasing severity of OA. Figure 2 demonstrates disease stages according to the KL grading system. While KL Grade 0 means no radiographic features of OA are present and it is normal, KL Grade 1 indicates presence of equivocal osteophyte. KL Grade 2 signifies presence of definite osteophyte and possible joint space narrowing (JSN). KL Grade 3 indicates presence of joint space narrowing, multiple osteophytes, and sclerosis. KL Grade 4 denotes complete loss of joint space, large osteophytes, severe sclerosis, and definitely bony deformity. International diagnostic threshold for radiographic OA is KL Grade 2: $KL < 2$ is defined as non-OA and $KL \geq 2$ is classified as OA. It is notable that KL grading suffers from significant inter

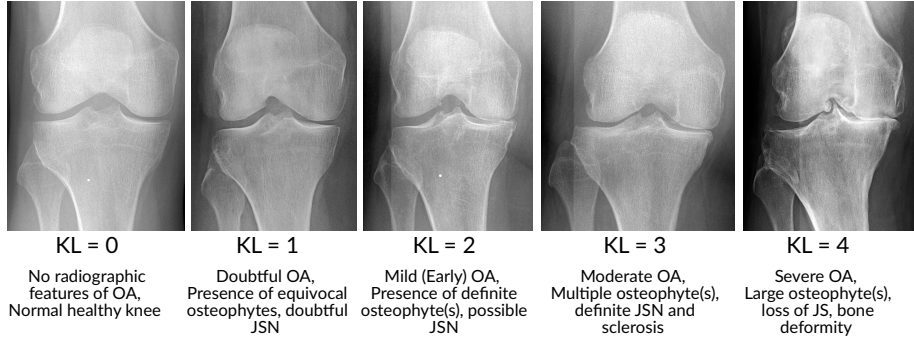


Fig. 2: Examples of knee X-Rays showing the stages of knee osteoarthritis severity according to KL grading. For the OA detection problem, $KL < 2$ is defined as non-OA and $KL \geq 2$ is classified as OA.

and intraobserver variation [6]. This is primarily due to subjective differences in interpretations of the X-ray features by observers and different study techniques.

It has been shown in several studies that OA severity assessment from radiographs can be enhanced using computer assisted methods [7–16]. Bone texture analysis is one of the main methodology in the automated analysis of knee radiographs [7, 9–11]. Bone shape analysis is another popular approach for OA detection [10, 17–19]. However, current state-of-the-art (SOTA) approaches for automatic OA detection and grading are based on machine learning techniques such as deep learning (DL) [12–14] and in particular deep convolutional neural networks (CNNs). The use of deep learning in OA research has been greatly increased in the last few years with the availability of large amounts of annotated data and computational processing power. However, these SOTA deep learning models suffer from significant shortcomings. Firstly, well known anatomical features associated with OA were not considered at all. For example, direct measurement of the separation between the distal femur and the proximal tibia, joint space width (**JSW**), which is the standard tool for the assessment of knee OA progression is not included [20]. Analysis of other radiographic hallmarks of primary OA including joint shape are also missing in these studies. Although deep features might cover some aspects of these anatomical features, the added value of explicit inclusion to the models have not been investigated. Moreover, in contrast to the common assumption, it was shown that CNNs rely extremely on textures and they perform poorly at recognising shapes without object texture [21]. Therefore, it is also important to study the outcomes when the bone shape representations are explicitly included. Second, existing models have huge number of parameters and compute redundant features due to blind region selection. However, it was found that in OA radiographically most distinctive bony changes occur at the medial tibia margin [22]. It was observed in [22] that this region of interest (ROI) has a profound effect on bone texture analysis. Existing methods usually resize whole knee joint images blindly for using well known

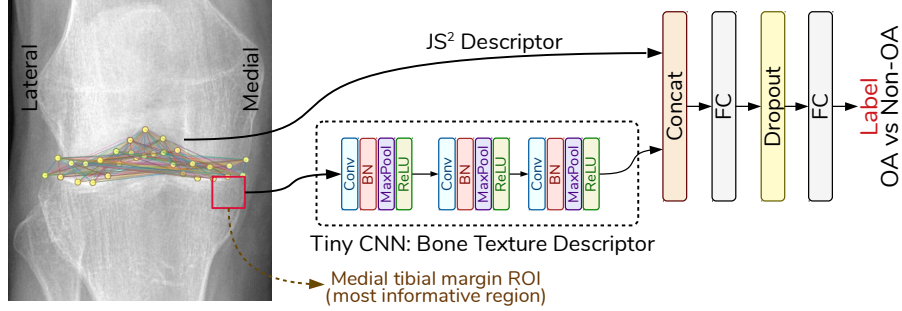


Fig. 3: We propose a model that combines bone shape and bone texture using a tiny CNN model to detect OA. Our novel joint shape and joint space JS^2 descriptor and lightweight CNN features complement each other.

CNN architectures (VGG, ResNet family, etc.) and take the advantage of transfer learning or fine tuning. These approaches comes at a price: computational power and substantial amount of labeled data for training. Lastly, such models are characteristically opaque, i.e., what information in the input data makes them to make their decisions is unclear.

In this study, we propose a model that combines bone shape and bone texture using a tiny CNN model to detect OA as defined by $KL \geq 2$. Firstly, we propose a compact joint shape and joint space (JS^2) descriptor that can be used as a marker of radiographic OA. Second, we explored whether deep texture features from the tibial margin in the medial side of the knee (the most informative region based on a recent study [22]) provides comparable results with the SOTA approaches in which the whole knee joint radiographs were analyzed. Employing a small ROI enables us to use tiny CNN models that are having significantly less parameters compared to current SOTA DL models and are efficient in terms of both data and computational complexity. Finally, we propose a novel model where both bone texture and joint shape description are combined.

2 Method

2.1 Joint Shape and Joint Space (JS^2) Descriptor

With the progression of OA, subchondral bone experiences changes in its structure and composition [23–25]. Previously, it has been shown that the global shape of the tibiofemoral joint is associated with the structural severity of OA [10, 18]. Joint shape descriptors based on statistical shape modeling have also been successfully employed for radiographic OA detection [10, 17].

In addition to global shape descriptors, loss of JSW measured between the adjacent bones (femur and tibia) of the knee, which is called Joint Space Narrowing (**JSN**), has been applied for longitudinal measurement of disease progression [26]. KL grading system is also incorporating assessment of joint space

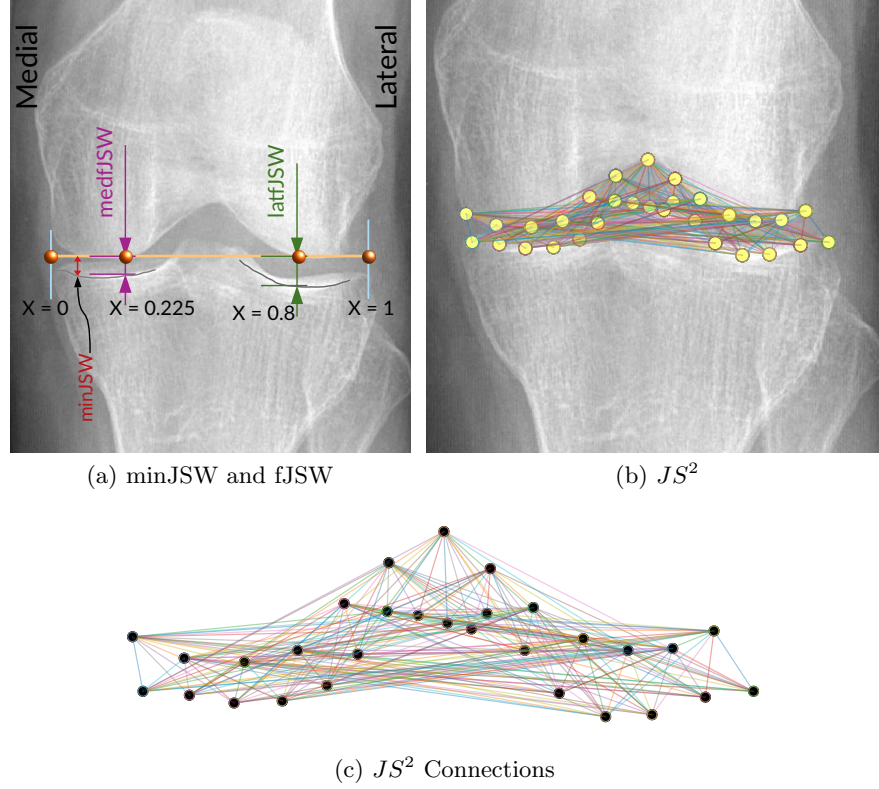


Fig. 4: (a) Illustration of joint space width (JSW) measurements at minimum (minJSW) and at fixed locations ($x = 0.225$ (medfJSW), $x = 0.8$ (latfJSW)). (b) Graphical illustration of our JS^2 descriptor on a sample knee radiograph. (c) JS^2 nodes and connections.

narrowing in addition to the osteophytes. Change in JSW has been considered a good measure of cartilage volume and thickness as well [27]. Therefore, minimum joint space width (**minJSW**) between the projected femur and tibia margins is the currently accepted metric to assess OA severity [20, 27]. However, the reproducibility of radiographic joint space measurements in longitudinal OA studies is problematic and not consistent [28]. Although previous studies have improved the reproducibility of minJSW by utilizing location-specific measurement of JSW (**fJSW**) [27, 29], JSW measurements do not necessarily translate into a change in radiographic grading of OA [28].

In this study, we propose a simple yet efficient descriptor to represent both shape of the knee joint and the spacing of tibiofemoral joint. Figure 4 and Algorithm 1 represent our proposed JS^2 descriptor. Our method is based on the anatomical landmarks in knee X-ray images and utilizes their spatial relations.

Algorithm 1: JS^2 descriptor

```

Tibia landmark points  $T_{pts} = t_0, t_1, t_2, \dots, t_{16}$ ;
Femur landmark points  $F_{pts} = f_0, f_1, f_2, \dots, f_{12}$ ;
 $k \leftarrow 0$ ;
for  $t_i$  in  $T_{pts}$  do
    for  $f_i$  in  $F_{pts}$  do
         $JS_k^2 = \|t_i - f_i\|$ ;
         $k \leftarrow k + 1$ ;
    end
end

```

Here, we utilized BoneFinder[®] software [30] in order to locate the landmark points along the contours of the distal femur and the proximal tibia (Figure 5). It uses random forest regression voting with constrained local model approach. Although, the BoneFinder[®] tool automatically locate 74 points, our JS^2 descriptor uses a total of 30 points (13 points on femur contour and 17 points at tibia contour) resulting a vector of length 221 (13×17) (see Figure 4) .

While previously adopted minJSW and fJSW [27, 29] measurements are used to assess JSN, our JS^2 descriptor translates joint shape, femur-tibia configuration and multiple JSW measurements together into a compact descriptor. Therefore, it can be directly utilized to detect radiographic OA.

2.2 Bone Texture Characterization

Recent study has considered OA as a whole-organ disease and suggest refocusing from solely cartilage-based studies to bone and other soft tissues together with the cartilage [31]. Since structural changes in subchondral bone occurs many months before changes in articular cartilage thickness (i.e. joint space narrowing) [23], there is a compelling interest towards detecting osteoarthritis with texture analysis of bone [8, 10].

Previous studies have reported significant differences in subchondral bone texture between controls and individuals with OA [7–9, 11, 22, 32]. However, subchondral bone remodelling in OA is not uniform. In OA, the bone closest to the articular cartilage experiences the greatest effect and damage. Therefore, alterations in subchondral bone texture are observed best at those regions and particularly at medial tibial compartment [22, 32, 33]. The rest of the bone do not reveal texture differences in radiographs in such detail [22]. Inspired by this phenomenon, rather than using the whole joint radiography we employed only the most informative region in our study (Figure 3). Here, we utilized again the landmark points to locate our ROI at medial tibia margin. We used a square patch with dimensions proportional to the width of the knee.

Previously, subchondral bone texture in the radiographs have been quantified mostly by fractal methods [9] and other conventional texture descriptors such as Local Binary Patterns [22]. This is the first study to evaluate OA texture

Table 1: Architecture of our tiny CNN. Each convolution layer (stride =1, padding =1) is followed by Batch normalization (BN), max pooling (2×2) and ReLU. For classification, we used two fully connected (FC) layers with dropout=0.5.

Layer	Output size	Architecture
Input	48×48	
Conv-1 + BN + MaxPool + ReLU	24×24	$[3 \times 3, 32]$
Conv-2 + BN + MaxPool + ReLU	12×12	$[3 \times 3, 64]$
Conv-3 + BN + MaxPool + ReLU	6×6	$[3 \times 3, 128]$

Table 2: Description of the data. We used data from the OAI dataset and MOST dataset at baseline with postero-anterior view with 10 degrees beam angle (PA10) of the knee given that both joints are graded with KL score. Missing entries were imputed and knees with total knee replacement were excluded.

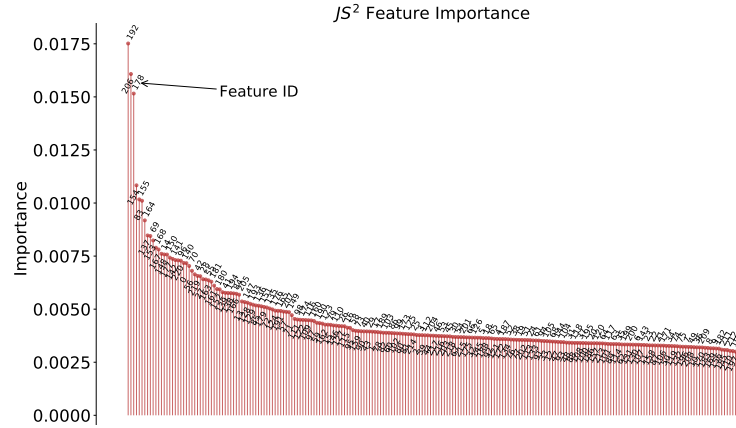
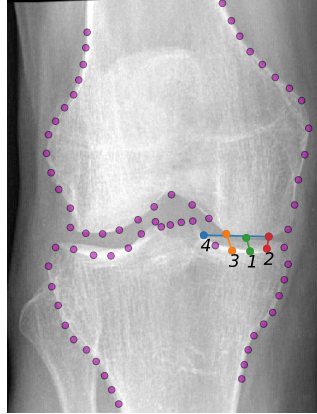
	OAI	MOST
	Train Data	Test Data
Number of knees	8953	3445
Number of subjects	4506	1748
Number of knees where $KL < 2$, (non-OA)	5045	2118
Number of knees where $KL \geq 2$, (OA)	3908	1327

using a CNN model. We extracted texture features using a simple three layers CNN model (see Table 1). The model is presented in Figure 3 (lower branch). Considering the heavy parameters of the current CNN-based methods in OA research that often use VGG or ResNets family as backbones [12–14], training from scratch is pretty difficult with limited training samples. Thanks to the lightweight architecture of our CNN model, it can be trained from scratch with a good convergence.

3 Experiments

We used the data from the Osteoarthritis Initiative (OAI, <http://www.oai.ucsf.edu/>) and Multicenter Osteoarthritis Study (MOST, <http://most.ucsf.edu>). We selected all knees at baseline that are graded by KL score on both knees. Missing entries were imputed and knees with total knee replacement were excluded. The details about OAI and MOST datasets used in this study are presented in Table 2. As a strength of our paper, we validated our trained model with an independent test set (MOST) that is completely different from the training set (OAI) similar to [14, 22].

Firstly, landmark points (keypoints) of knee radiographs were extracted using an open software BoneFinder[®] [30]. In the preprocessing pipeline, the 16-bit DICOM images are first normalized using global contrast normalisation and histogram truncation between the 5th and 99th percentiles and then converted to 8-bit images. The resolution, which is not initially standardized in the database,

(a) Feature Importance of JS^2 

(b)

Fig. 5: Figure (a) shows the feature importance of JS^2 and (b) illustrates sample knee joint radiograph with landmarks and the most important four features of our JS^2 descriptor.

is also standardized to 0.2 mm. Finally, using landmark points, each knee is rotated in order to have an aligned horizontal tibial plateau. Subsequently, for texture characterization, we cropped a square patch having a side length of $1/7^{th}$ of the knee tibia width. Before feeding this texture ROI to our tiny CNN, it was rescaled to 56×56 pixels and random 48×48 pixel crops were then employed.

3.1 Reference Methods

We used several reference methods to compare with the proposed approach. For texture analysis, we employed LBP [34], Fractal Dimension (FD) [35, 36], Bilinear CNN (B-CNN) [37] and anti-aliased CNN [38]. Modern CNNs are not shift

invariant and drastic changes at the networks output can be observed due to one pixel shift of an input image. One possible solution is to use the antialiased networks [38] which utilizes signal processing technique (low-pass filtering before downsampling) to fix this. We also tested B-CNN that captures pairwise correlations between the feature channels and showed promising results in fine-grained (texture) recognition problems [37].

For shape-based analysis, we compared minJSW and fJSW which are commonly used in OA research [27, 29]. Locations of fJSW measurements are illustrated in Figure 4 in which the knee joint is first aligned with respect to femur (i.e. x-axis is aligned with femoral condyles in both compartments). The y-axis of the coordinate system is defined as the peripheral edge of the femoral condyle. Subsequently, the fixed locations are selected at $x = 0.225$ (medialfJSW) and $x = 0.8$ (lateral fJSW) following the literature [27, 29]. These measurements are adjusted with respect to the tibia width. Reference models based on LBP, FD, minJSW and fJSW were assessed using Logistic Regression (LR) with ' L_2 ' regularization using scikit-learn package [39].

3.2 Model, Training and Parameter Settings

Our CNN model consists of 3 convolutional layers dedicated to texture feature extraction. Each convolution layer (stride=1, padding=1) is followed by Batch normalization (BN), max pooling (2×2) and ReLU. In our CNN-based experiments, we used two fully connected layers to make the prediction. A dropout of 0.5 is inserted after the first fully connected layer. For the combined model, where we concatenated shape and texture features, we adopted dropout of 0.3 as it provides better performance.

In all the experiments, we used the same training strategy. We trained the models from scratch (end-to-end) using the random weight initialization. We adopted stochastic gradient descent training on a GPU. A mini-batch of 64 images were employed, and a momentum of 0.9 was used and trained without weight decay. We used a starting learning rate of 0.01 and decreased it by 10 every 8 epochs. The models were trained for 100 epochs and we selected the model with a best performance. Therefore, our results present an upper bound (Table 3). We trained our tiny CNN model also with data augmentations where we used small random rotations, gamma and brightness corrections. However, it did not improve the scores. This could be due to the knee alignment and pre-processing, which we performed before the ROI extraction.

For assessing the JS^2 descriptor we used both LR and two layer neural network (NN) which is similar to the last fully connected layers in the tiny CNN model. We used PyTorch v1.4 in our experiments [40].

3.3 Results

In Table 3, we present the area under the receiver operating characteristic curves (ROC AUC) to measure classifier performance effectively.

Table 3: Comparison of the models’ performance in detecting radiographic OA ($KL \geq 2$). Reference models were assessed using Logistic Regression (LR). Here, Area under the ROC curve (AUC) metric is used for assessment. NN: Neural Network.

	Method	ROC AUC (%)
Texture	LBP (LR)	82.69
	Fractal Dimension (LR)	74.80
	CNN	88.74
	B-CNN [37]	88.53
	Anti-alised CNN [38]	87.93
Morphology	minJSW (LR)	70.74
	minJSW + medfJSW + latfJSW (LR)	81.75
	JS^2 Descriptor (LR) (ours)	91.18
	JS^2 Descriptor (NN) (ours)	93.52
	JS^2 Descriptor	93.60
	+ minJSW + medfJSW + latfJSW (NN)	
Combined	JS^2 Descriptor + CNN (ours)	95.21

Texture characterization. We found that compared to the conventional methods, CNN-based texture extraction leads to better performance in detecting radiographic OA. However, B-CNN and anti-alised CNN models did not improve the performance further. Compared to the hand-crafted features, a plain tiny CNN model outperforms the best reference method by 6%.

Joint Space - Joint Shape. In this study, we evaluated minJSW for incident OA detection. Then we combined minJSW measurement with JSW measurements at fixed locations (fJSW), which improved the performance roughly 11%. The ROC AUC value achieved by our JS^2 method was 93.52% which is significantly better than other approaches. In addition to the classifier performances, we investigated the feature importance of JS^2 (Figure 5). Feature importance was calculated based on forests of trees classifier using scikit-learn package [39]. Figure 5a illustrates how much each feature contributes to the model’s overall predictive performance. Most of the features are equally informative and, therefore, they cannot be ignored. Figure 5b illustrates the first four most important elements of JS^2 . Interestingly, the fourth one might be related to knee alignment. We evaluated the distribution of the most important JS^2 feature. Figure 6 demonstrates the density plot of the most important feature for OA and non-OA cases. The mean (std) value of $JS^2[192]$ is $3.98mm(std\ 1.57mm)$ for OA and $5.17mm(std\ 0.96mm)$ for non-OA. Although not presented here, other features demonstrate similar characteristics. Finally, we evaluated the robustness of our descriptor to JSW measurement errors and variability. The sources of errors and variability could be due to positioning accuracy in the acquisition of clinical knee X-rays and the landmark extraction method. In order to simulate this, we added Gaussian distributed noise to our

JS^2 descriptor with zero mean and standard deviation of 1mm, 3mm and 5mm to both train and test data. Table 4 demonstrates that our model is not sensitive to noisy JSW measurements.

To evaluate the true additive value of our JS^2 descriptor in the combined model, we assessed the descriptor’s predictive ability both with LR and NN (Table 3).

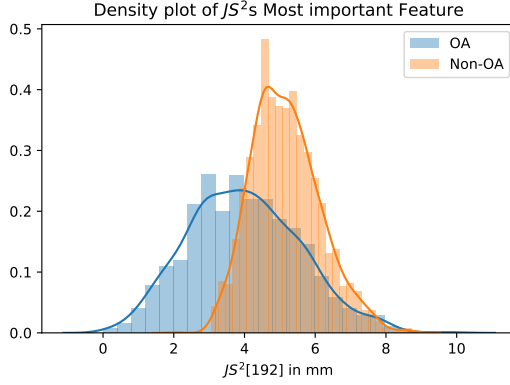


Fig. 6: Figure shows the density plot of $JS^2[192]$ feature which is the most important element in the descriptor.

Combined model As mentioned previously, we combined CNN-based texture features and our JS^2 descriptor to form a single vector and trained our classifier on fused feature (Figure 3). This model performed better than both texture and shape based models (ROC AUC = 95.21%). This finding suggests that bone texture and joint shape carry complementary information for automatic detection of radiographic OA. The closest work to ours is Thomson et al. [10] where they also combined shape and texture descriptors to detect OA. They reported 85% ROC AUC using direct pixel ratios as texture descriptor and shape parameter vectors obtained from statistical shape modelling. Moreover, our combined model achieves classification performance comparable, if not better, than the SOTA DL-based OA detection models [12, 14].

Table 4: Analysis of detection performance in case of noisy JS^2 measurements. Gaussian noise with zero mean is added to the JS^2 vector.

Model	ROC AUC (%)					
	Noise Std		Noise Std		Noise Std	
	1mm	3mm	5mm	1mm	3mm	5mm
JS^2	93.21	92.51	91.81			
Combined (JS^2 + CNN)	94.85	94.58	94.17			

4 Discussions and Conclusions

In this study, we propose a simple knee joint shape descriptor JS^2 for OA detection from plain radiographs. In addition, we demonstrated that a lightweight CNN for extracting bone texture features together with our proposed joint shape-joint space descriptor achieves SOTA performance in radiographic OA detection. Moreover, we evaluated the most important JS^2 features that contribute to OA presence. Unlike existing black-box deep CNN based models in the field, our descriptor provides more explainable results that translate features to an important structural change in joint anatomy that may contribute to OA. We also demonstrated that our proposed JS^2 descriptor is robust to noisy joint space width measurements.

In our tiny CNN model, we utilized the most informative ROI (a very small image patch which is cropped from the medial tibia margin) to build a network with fewer parameters. Compared to the heavy deep CNN models that use whole joint image, our tiny model still has the ability to recognize OA with high accuracy. Our CNN model yields the highest score among the all previously published texture-based methods [22].

This study has also some limitations. First, our proposed descriptor is based on landmarks that needs to be extracted beforehand and this brings a preprocessing overhead. However, similar overhead is also present in SOTA DL approaches for detecting the joint ROI from the full limb radiographs. Second, although medial OA is more common, other bone compartments (such as lateral and femur margins) which might hold new/complementary information of OA were not evaluated in our study. Their inclusion could further improve the performance, which could be further investigated. Admittedly, the models which utilize whole joint radiographs have the potential to utilize those features as a rule. Therefore, they are potentially better suited for fine-grained KL classification (KL 0, 1, 2, 3, and 4).

This study provides two important topics for future investigations. Firstly, fusing the proposed shape descriptor with the existing deep learning models to evaluate whether they capture shape-related features inherently or their performance can be improved by the explicit inclusion of shape features. Secondly, predicting the progression of OA using JS^2 descriptor. Apart from OA, we believe that JS^2 descriptor could be useful in other fields where joint space features are important in disease assessment such as rheumatoid arthritis. Our source codes are available at <https://github.com/MIPT-Oulu/JS2>.

Acknowledgments

The OAI is a public-private partnership comprised of five contracts (N01-AR-2-2258; N01-AR-2-2259; N01-AR-2-2260; N01-AR-2-2261; N01-AR-2-2262) funded by the National Institutes of Health, a branch of the Department of Health and Human Services, and conducted by the OAI Study Investigators. Private funding partners include Merck Research Laboratories; Novartis Pharmaceuticals

Corporation, GlaxoSmithKline; and Pfizer, Inc. Private sector funding for the OAI is managed by the Foundation for the National Institutes of Health. This manuscript was prepared using an OAI public use data set and does not necessarily reflect the opinions or views of the OAI investigators, the NIH, or the private funding partners

Multicenter Osteoarthritis Study (MOST) Funding Acknowledgment. MOST is comprised of four cooperative grants (Felson AG18820; Torner AG18832, Lewis AG18947, and Nevitt AG19069) funded by the National Institutes of Health, a branch of the Department of Health and Human Services, and conducted by MOST study investigators. This manuscript was prepared using MOST data and does not necessarily reflect the opinions or views of MOST investigators.

We would like to acknowledge the strategic funding of the University of Oulu, Infotech Oulu.

We gratefully acknowledge the help received from Aleksei Tiulpin who extracted the landmarks using BoneFinder[®] and the support of NVIDIA Corporation with the donation of the Quadro P6000 GPU used in this research.

References

1. J. W. Bijlsma, F. Berenbaum, and F. P. Lafeber, "Osteoarthritis: an update with relevance for clinical practice," *The Lancet*, vol. 377, no. 9783, pp. 2115–2126, 2011.
2. R. D. Altman, "Early management of osteoarthritis," *The American journal of managed care*, vol. 16, pp. S41–7, 2010.
3. B. Heidari, "Knee osteoarthritis prevalence, risk factors, pathogenesis and features: Part i," *Caspian journal of internal medicine*, vol. 2, no. 2, p. 205, 2011.
4. I. Haq, E. Murphy, and J. Dacre, "Osteoarthritis," *Postgraduate Medical Journal*, vol. 79, no. 933, pp. 377–383, 2003.
5. J. Kellgren and J. Lawrence, "Radiological assessment of osteoarthrosis," *Annals of the rheumatic diseases*, vol. 16, no. 4, p. 494, 1957.
6. Ö. Köse, B. Acar, F. Çay, B. Yilmaz, F. Güler, and H. Y. Yüksel, "Inter-and intraobserver reliabilities of four different radiographic grading scales of osteoarthritis of the knee joint," *The journal of knee surgery*, vol. 3, no. 03, pp. 247–253, 2018.
7. J. Lynch, D. Hawkes, and J. Buckland-Wright, "Analysis of texture in macro-radiographs of osteoarthritic knees, using the fractal signature," *Physics in Medicine & Biology*, vol. 36, no. 6, p. 709, 1991.
8. V. B. Kraus, J. E. Collins, H. C. Charles, C. F. Pieper, L. Whitley, E. Losina, M. Nevitt, S. Hoffmann, F. Roemer, A. Guermazi, *et al.*, "Predictive validity of radiographic trabecular bone texture in knee osteoarthritis: the osteoarthritis research society international/foundation for the national institutes of health osteoarthritis biomarkers consortium," *Arthritis & Rheumatology*, vol. 70, no. 1, pp. 80–87, 2018.
9. J. Hirvasniemi, J. Thevenot, V. Immonen, T. Liikavainio, P. Pulkkinen, T. Jämsä, J. Arokoski, and S. Saarakkala, "Quantification of differences in bone texture from plain radiographs in knees with and without osteoarthritis," *Osteoarthritis and cartilage*, vol. 22, no. 10, pp. 1724–1731, 2014.

10. J. Thomson, T. O'Neill, D. Felson, and T. Cootes, "Automated shape and texture analysis for detection of osteoarthritis from radiographs of the knee," in *International Conference on Medical Image Computing and Computer-Assisted Intervention*, pp. 127–134, Springer, 2015.
11. T. Janvier, R. Jennane, H. Toumi, and E. Lespessailles, "Subchondral tibial bone texture predicts the incidence of radiographic knee osteoarthritis: data from the osteoarthritis initiative," *Osteoarthritis and cartilage*, vol. 25, no. 12, pp. 2047–2054, 2017.
12. J. Antony, K. McGuinness, N. E. O'Connor, and K. Moran, "Quantifying radiographic knee osteoarthritis severity using deep convolutional neural networks," in *Pattern Recognition (ICPR), 2016 23rd International Conference on*, pp. 1195–1200, IEEE, 2016.
13. B. Norman, V. Pedoia, A. Noworolski, T. M. Link, and S. Majumdar, "Applying densely connected convolutional neural networks for staging osteoarthritis severity from plain radiographs," *Journal of digital imaging*, vol. 32, no. 3, pp. 471–477, 2019.
14. A. Tiulpin, J. Thevenot, E. Rahtu, P. Lehenkari, and S. Saarakkala, "Automatic knee osteoarthritis diagnosis from plain radiographs: a deep learning-based approach," *Scientific reports*, vol. 8, no. 1, p. 1727, 2018.
15. M. Górriz, J. Antony, K. McGuinness, X. Giró-i Nieto, and N. E. O'Connor, "Assessing knee oa severity with cnn attention-based end-to-end architectures," in *International Conference on Medical Imaging with Deep Learning*, pp. 197–214, 2019.
16. J. Abedin, J. Antony, K. McGuinness, K. Moran, N. E. O'Connor, D. Reibholz-Schuhmann, and J. Newell, "Predicting knee osteoarthritis severity: comparative modeling based on patients data and plain x-ray images," *Scientific reports*, vol. 9, no. 1, pp. 1–11, 2019.
17. L. Minciullo and T. Cootes, "Fully automated shape analysis for detection of osteoarthritis from lateral knee radiographs," in *Pattern Recognition (ICPR), 2016 23rd International Conference on*, pp. 3787–3791, IEEE, 2016.
18. D. J. Haverkamp, D. Schiphof, S. M. Bierma-Zeestra, H. Weinans, and J. H. Waarsing, "Variation in joint shape of osteoarthritic knees," *Arthritis & Rheumatism*, vol. 63, no. 11, pp. 3401–3407, 2011.
19. A. M. Martinez, I. Flament, F. Liu, J. Lee, P. Cao, S. Majumdar, and V. Pedoia, "Discovering knee osteoarthritis bone shape features using deep learning," *Osteoarthritis and Cartilage*, vol. 27, pp. S386–S387, 2019.
20. S. Ahlback, "Osteoarthrosis of the knee. a radiographic investigation," *Acta radiol.*, vol. 227, pp. 7–72, 1968.
21. R. Geirhos, P. Rubisch, C. Michaelis, M. Bethge, F. A. Wichmann, and W. Brendel, "Imagenet-trained cnns are biased towards texture; increasing shape bias improves accuracy and robustness," *arXiv preprint arXiv:1811.12231*, 2018.
22. N. Bayramoglu, A. Tiulpin, J. Hirvasniemi, M. T. Nieminen, and S. Saarakkala, "Adaptive segmentation of knee radiographs for selecting the optimal roi in texture analysis," *Osteoarthritis and Cartilage*, 2020.
23. C. Buckland-Wright, "Subchondral bone changes in hand and knee osteoarthritis detected by radiography," *Osteoarthritis and cartilage*, vol. 12, pp. 10–19, 2004.
24. L. Kamibayashi, U. Wyss, T. Cooke, and B. Zee, "Trabecular microstructure in the medial condyle of the proximal tibia of patients with knee osteoarthritis," *Bone*, vol. 17, no. 1, pp. 27–35, 1995.
25. S. R. Goldring, "Role of bone in osteoarthritis pathogenesis," *Medical Clinics of North America*, vol. 93, no. 1, pp. 25–35, 2009.

26. N. Mehta, J. Duryea, G. J. Badger, M. R. Akelman, M. H. Jones, K. P. Spindler, and B. C. Fleming, "Comparison of 2 radiographic techniques for measurement of tibiofemoral joint space width," *Orthopaedic journal of sports medicine*, vol. 5, no. 9, p. 2325967117728675, 2017.
27. G. Neumann, D. Hunter, M. Nevitt, L. Chibnik, K. Kwoh, H. Chen, T. Harris, S. Satterfield, J. Duryea, *et al.*, "Location specific radiographic joint space width for osteoarthritis progression," *Osteoarthritis and cartilage*, vol. 17, no. 6, pp. 761–765, 2009.
28. A. Guermazi, D. J. Hunter, and F. W. Roemer, "Plain radiography and magnetic resonance imaging diagnostics in osteoarthritis: validated staging and scoring," *JBJS*, vol. 91, no. Supplement_1, pp. 54–62, 2009.
29. J. Duryea, S. Zaim, and H. Genant, "New radiographic-based surrogate outcome measures for osteoarthritis of the knee," *Osteoarthritis and cartilage*, vol. 11, no. 2, pp. 102–110, 2003.
30. C. Lindner, S. Thiagarajah, J. M. Wilkinson, G. A. Wallis, T. F. Cootes, arcOGEN Consortium, *et al.*, "Fully automatic segmentation of the proximal femur using random forest regression voting," *IEEE transactions on medical imaging*, vol. 32, no. 8, pp. 1462–1472, 2013.
31. R. M. Aspden and F. Saunders, "Osteoarthritis as an organ disease: from the cradle to the grave," *European cells & materials*, 2019.
32. J. W. MacKay, P. J. Murray, B. Kasmai, G. Johnson, S. T. Donell, and A. P. Toms, "Subchondral bone in osteoarthritis: association between mri texture analysis and histomorphometry," *Osteoarthritis and cartilage*, vol. 25, no. 5, pp. 700–707, 2017.
33. T. Janvier, H. Toumi, K. Harrar, E. Lespessailles, and R. Jennane, "Roi impact on the characterization of knee osteoarthritis using fractal analysis," in *Image Processing Theory, Tools and Applications (IPTA), 2015 International Conference on*, pp. 304–308, IEEE, 2015.
34. T. Ojala, M. Pietikäinen, and T. Mäenpää, "Gray scale and rotation invariant texture classification with local binary patterns," in *European Conference on Computer Vision*, pp. 404–420, Springer, 2000.
35. J. Lynch, D. Hawkes, and J. Buckland-Wright, "A robust and accurate method for calculating the fractal signature of texture in macroradiographs of osteoarthritic knees," *Medical Informatics*, vol. 16, no. 2, pp. 241–251, 1991.
36. J. Hirvasniemi, J. Thevenot, H. T. Kokkonen, M. A. Finnilä, M. S. Venäläinen, T. Jämsä, R. K. Korhonen, J. Töyräs, and S. Saarakkala, "Correlation of subchondral bone density and structure from plain radiographs with micro computed tomography ex vivo," *Annals of biomedical engineering*, vol. 44, no. 5, pp. 1698–1709, 2016.
37. T.-Y. Lin and S. Maji, "Improved Bilinear Pooling with CNNs," in *BMVC*, 2017.
38. R. Zhang, "Making convolutional networks shift-invariant again," *arXiv preprint arXiv:1904.11486*, 2019.
39. F. Pedregosa, G. Varoquaux, A. Gramfort, V. Michel, B. Thirion, O. Grisel, M. Blondel, P. Prettenhofer, R. Weiss, V. Dubourg, J. Vanderplas, A. Passos, D. Cournapeau, M. Brucher, M. Perrot, and E. Duchesnay, "Scikit-learn: Machine learning in Python," *Journal of Machine Learning Research*, vol. 12, pp. 2825–2830, 2011.
40. A. Paszke, S. Gross, F. Massa, A. Lerer, J. Bradbury, G. Chanan, T. Killeen, Z. Lin, N. Gimeshein, L. Antiga, *et al.*, "Pytorch: An imperative style, high-performance deep learning library," in *Advances in NIPS*, pp. 8024–8035, 2019.